

Lost in Transmission: On the Impact of Networking Corruptions on Video Machine Learning Models

Trenton Chang
University of Michigan
ctrenton@umich.edu

Daniel Y. Fu
Stanford University
danfu@cs.stanford.edu

Abstract

We study how *networking corruptions*—data corruptions caused by networking errors—affect video machine learning (ML) models. We discover apparent networking corruptions in Kinetics-400, a benchmark video ML dataset. In a simulation study, we investigate (1) what artifacts networking corruptions cause, (2) how such artifacts affect ML models, and (3) whether standard robustness methods can mitigate their negative effects. We find that networking corruptions cause visual and temporal artifacts (i.e., smeared colors or frame drops). These networking corruptions degrade performance on a variety of video ML tasks, but effects vary by task and dataset, depending on how much temporal context the tasks require. Lastly, we evaluate data augmentation—a standard defense for data corruptions—but find that it does not recover performance.

1 Introduction

Video machine learning (ML) models are known to be vulnerable against data corruptions. For example, sensor noise (e.g. color shift, blur) and environmental shifts (e.g. snow) [16, 17] can degrade model performance. Corruptions due to networking errors during data transmission—which we call *networking corruptions*—are relatively understudied in the literature. However, we find previously-undocumented instances of apparent networking corruptions in Kinetics-400, a benchmark video dataset. These corruptions appear qualitatively different from data corruptions. Understanding the impacts of such errors may reveal insights on what information is critical for video ML models. This understanding may also be increasingly relevant to video ML deployments, especially those distributed across networks [46, 47].

Understanding how networking corruptions impact video ML models is challenging. To begin, in contrast to data corruptions, networking corruptions can have complex downstream effects on videos. Networking corruptions can cause artifacts such as color smearing or dropped frames, even when the degree of data corruption is relatively small (Figure 1). Furthermore, video ML models are used for a variety of downstream applications, ranging from action recognition (classifying the action of a single video), to per-frame object segmentation. As a result, it is unclear how these artifacts impact video ML tasks—for example, smearing artifacts may impact object segmentation differently than action recognition.

In this paper, we study the impact of networking corruptions on video ML models through a simulation study. First, we qualitatively investigate the impact of networking corruptions on videos

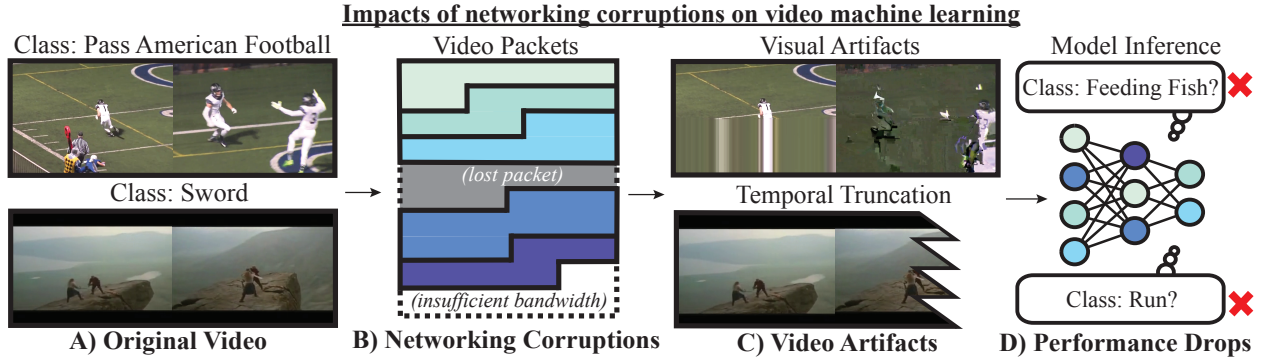


Figure 1: Network issues during video transmission can cause *networking corruptions*, which cause visual artifacts such as color smearing and temporal artifacts such as dropped frames. These corruptions degrade the performance of video ML models during inference.

(Section 3). We describe two artifact types: (1) visual artifacts, which fill frames with transient visual noise, and (2) temporal truncation, which drops frames from the end of the video. We find that these artifact types are correlated with high packet loss rate and low bandwidth limitations, respectively.

Next, we assess how these artifacts impact four video ML tasks: action recognition, object tracking, object segmentation, and captioning (Section 4). Networking corruptions degrade performance across tasks (up to 46.0% accuracy on Kinetics-400), but effects vary by task and dataset. For example, temporal truncation lowers action recognition accuracy, but has little impact on object tracking. We characterize these impacts, and provide guidance on which tasks are affected by which artifacts based on how much temporal context they require.

Lastly, we evaluate whether data augmentation, a standard robustness technique, recovers performance under networking corruptions (Section 5). Although data augmentation may offer minor protection against strong visual artifacts (+3.0% accuracy), it has trouble adapting to truncation. We also evaluate a broader suite of defenses (Appendix C), but find that none can fully recover performance. Targeting specific artifact types is a potential direction for future work.

1.1 Preliminaries: Video Encoding and Transmission

First, we provide background on video encoding and transmission.

In this paper, we focus on the popular H.264 codec [33] (we report experiments with an alternate codec in Appendix C). H.264 exploits visual redundancy between frames by storing a few full frames called *keyframes*. The remaining frames store differences with respect to previous frames. Frame data is then compressed via quantization and entropy encoding. H.264 also uses error concealment and correction to mitigate bitstream errors [37].

To transmit video, the video bitstream is chunked into network packets that contain frames or partial frames. These are transmitted via a network link, then decoded for downstream use (e.g. ML model inference). Networking corruptions may corrupt/delete portions of the bitstream; even small data losses can cause artifacts or render the video unplayable.

2 Networking Corruptions in Kinetics-400

We describe apparent networking corruptions found in the Kinetics-400 action recognition dataset. These corruptions appear as visual artifacts (i.e. blocky pixels, smearing), and differ from corruptions



Figure 2: Visual artifacts from apparent networking corruptions in Kinetics-400.

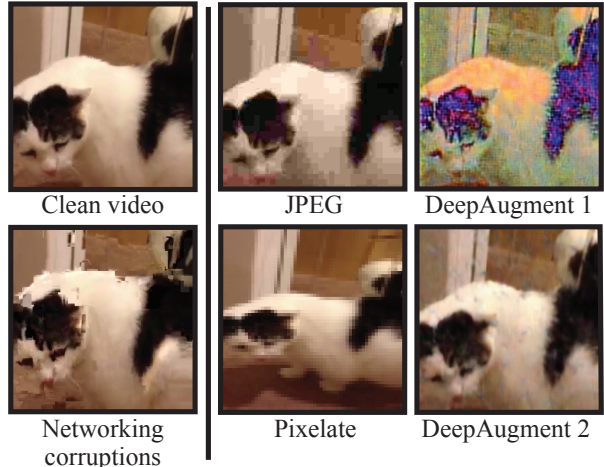


Figure 3: Networking corruptions appear qualitatively different from data corruptions in ImageNet-C and -R. **Top left:** Clean video. **Bottom left:** Video under networking corruptions (simulated). **Middle:** JPEG compression and pixelation from ImageNet-C. **Right:** Two realizations of DeepAugment [15].

in existing image robustness benchmarks. Corruptions were found by manually looking for visible artifacts in a random sample of 400 Kinetics-400 videos.

Figure 2 shows frames with apparent networking corruptions from Kinetics-400. Each frame contains “blocky” artifacts: in a wrestler’s shadow (top left), the top of a floor mat (top right), a baby’s head (bottom left), and a person’s hand (bottom right). These artifacts move frame-to-frame, tracking with motion in the video. This is likely a *keyframe* corruption, which can cause visual artifacts. Applying additional frame differences (i.e., subsequent non-keyframes) would cause the artifacts to move, as observed.

Networking corruptions also appear different from well-studied visual data corruptions. Figure 3 compares networking corruptions to those in the ImageNet-C and -R [15, 16] robustness benchmarks. While networking corruptions cause local artifacts and visual discontinuities, ImageNet-C and -R corruptions are visually consistent across the frame. Networking corruption artifacts also change visually over time—a failure mode unique to videos.

3 Impacts on Videos

Motivated by our empirical findings, we conduct a simulation study of networking corruptions. We confirm networking corruptions cause visual artifacts similar to those in Kinetics-400. We also find that networking corruptions cause temporal artifacts (e.g. temporal truncation). Furthermore, we find that visual and temporal artifacts are correlated with specific network failure modes: high packet loss and low bandwidth.

Datasets We use seven video datasets from four ML tasks with various video lengths, sources (i.e. home video vs. TV), and resolutions. For action recognition, we use HMDB51 [24], UCF101 [36], Kinetics-400 [21], and SomethingSomething-V2 (SSV2) [13]. For single-object tracking, we use OTB-2015 [41]. For video object segmentation, we use DAVIS2017 [31]. For video captioning, we use MSR-VTT [42].

Simulation Method We stream videos in real-time from one machine to itself via an emulated

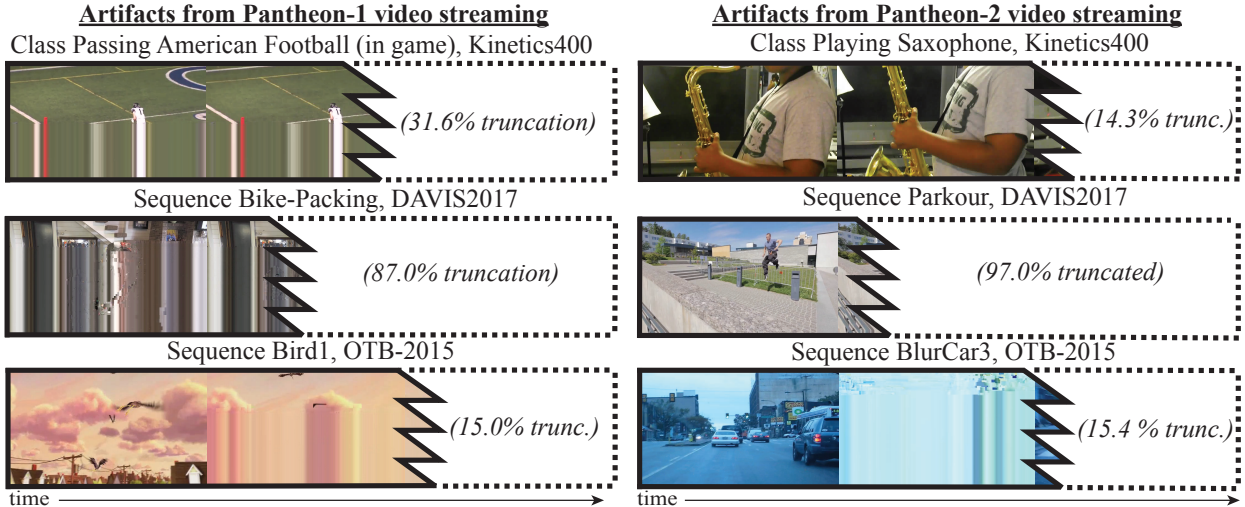


Figure 4: Visual artifacts and temporal truncation (not to scale) from streaming via Pantheon-1 (*left*) and -2 (*right*) on Kinetics-400 (*top*), DAVIS (*middle*), and OTB-2015 (*bottom*). Pantheon-1 causes visual artifacts and temporal truncation. Pantheon-2 typically causes temporal truncation, but occasionally causes visual artifacts (i.e. smears in bottom right).

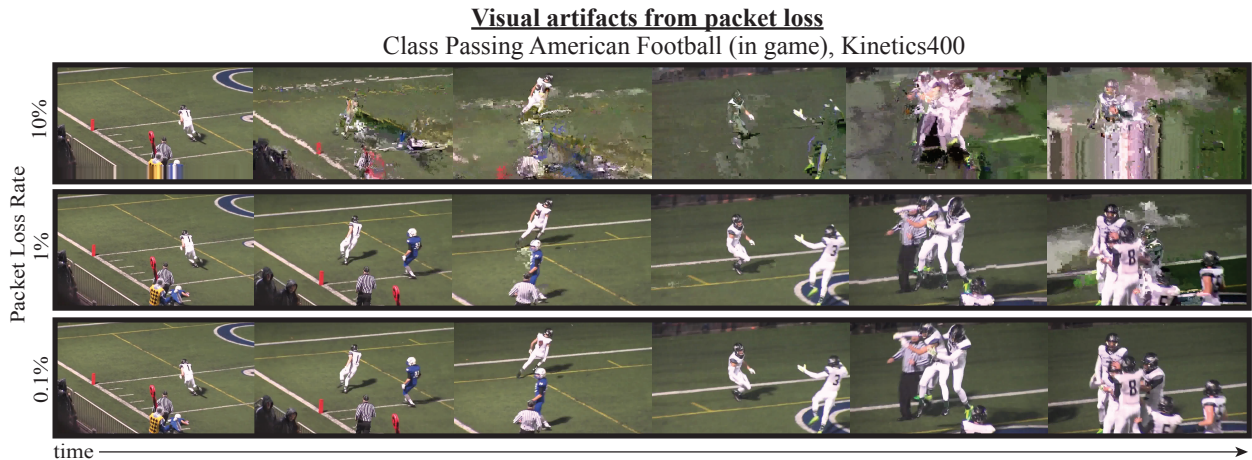


Figure 5: Visual artifacts from a Kinetics-400 video under 10% (*top*), 1% (*middle*), and 0.1% (*bottom*) packet loss. Higher packet loss worsens visual artifacts.

UDP link. Table 1 describes the network links we simulate. These parameters are taken from the Pantheon networking benchmark [44], which contains network conditions calibrated to empirically-measured network behavior.

Each link has five network parameters: (1) packet loss rate p (%), the % of packets dropped during transmission, (2) bandwidth B (megabits per second/Mbps), (3) whether packet arrival times are time-varying, (4) delay t (milliseconds), and (5) queue size S (# of packets), the number of packets the receiver can hold for post-processing before dropping packets.

3.1 Networking Corruption Artifacts

We investigate how networking corruptions impact videos. We describe two types of artifacts: visual artifacts and temporal truncation. Visual artifacts are correlated with high packet loss; temporal truncation is correlated with low bandwidth.

Table 1: Network Link Settings from Pantheon for Simulating Networking Corruptions (left to right: p =% packet loss rate, B =bandwidth in Mbps, usage of time-varying packet arrivals, t =delay in ms, S =queue size in # of packets).

Network link name	p	B (Mbps)	Time-Var.	t (ms)	S
Pantheon-1 (Nepal → AWS India, Wi-Fi)	4.77	0.57	Y	28	14
Pantheon-2 (Mexico → AWS California, Cellular)	0	2.64	Y	88	130
Pantheon-3 (AWS Brazil → Colombia, Cellular)	0	3.04	Y	130	426
Pantheon-4 (India → AWS India, Wired)	0	100.42	N	27	173

Pantheon-1 causes visual artifacts and temporal truncation Figure 4 (left) shows artifacts from Pantheon-1 on HMDB51, DAVIS, and OTB-2015. Pantheon-1 causes visual artifacts and temporal truncation. The visual artifacts appear as smearing, color bands, or blocky pixels that change frame-to-frame. Such artifacts are likely due to *keyframe* corruptions—errors in encoded full frames. Applying encoded frame differences to a corrupted keyframe spreads artifacts to subsequent frames. Temporal truncation drops frames from the end of the video. This disproportionately impacts datasets with shorter videos: median video length drops from 2.67s to 0.60s (-77.5%) on HMDB51, and from 4.17s to 0.08s (-98.0%) on SSV2—almost the entire video is lost. Remaining frames often contain visual artifacts.

Pantheon-2 and -3 cause temporal truncation and occasional visual artifacts Figure 4 (right) shows artifacts from Pantheon-2 on HMDB51, DAVIS, and OTB-2015. In some cases, video frames are missing, but the remaining frames are free of visual artifacts. On Kinetics-400, Pantheon-2 and -3 cut median video length from 10.0s to 8.44s (-15.6%) and 8.51s (-14.9%) respectively, but the remaining frames appear “clean” (Figure 4 top right). In other cases (particularly OTB-2015), visual artifacts occur in addition to temporal truncation (note color smears, Figure 4 bottom right).

Pantheon-4 sometimes causes minor visual artifacts and temporal truncation Pantheon-4 has little impact on videos. In a sample of 400 videos, small visual artifacts appeared briefly in a minority of videos. Temporal truncation is minor; video length drops at most 0.85s (DAVIS).

High packet loss is correlated with visual artifacts; low bandwidth is correlated with temporal truncation. To investigate why visual artifacts and temporal truncation emerge when streaming, we stream videos via simulated network links in which only packet loss rate and bandwidth vary. Appendix B reports results for other networking variables; we do not find strong correlations with video artifacts.

High packet loss rate is correlated with visual artifacts (Figure 5), while limiting bandwidth worsens temporal truncation (Figure 6). This is consistent with the artifacts seen on Pantheon links. Pantheon-1, which consistently causes visual artifacts, is the only link with a nonzero packet loss rate. Pantheon-1 through -3, which cause temporal truncation, have bandwidths much lower than that of Pantheon-4 (100.42Mbps), where we observed minor truncation.

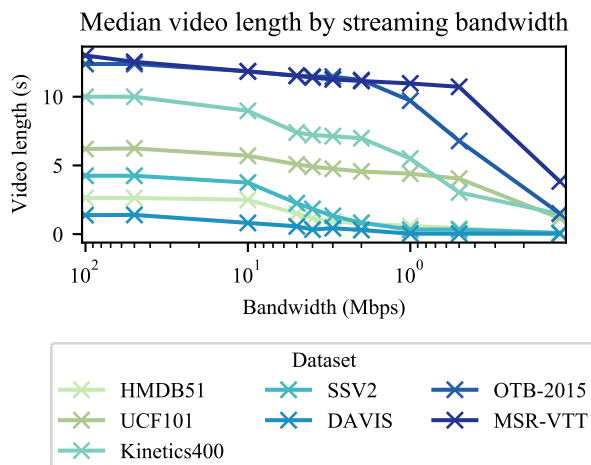


Figure 6: Median video length (*in seconds*) vs. bandwidth. Bandwidth limits can truncate the video.

Table 2: Summary of Impacts of Networking Corruptions

Task	Output frequency	Visual artifact impacts	Temporal truncation impacts
Action Recognition	Per-video	Performance drops	Perf. drops (if temporal context required)
Object Tracking	Per-frame	Performance drops	Inflated performance
Object Segmentation	Per-frame	Performance drops	Inflated performance
Video Captioning	Per-video	Small perf. drop; captions change	Captions change

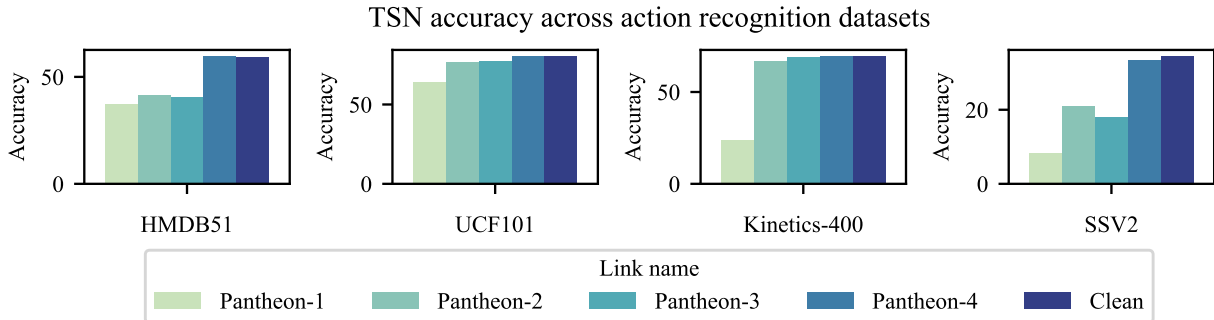


Figure 7: TSN accuracy on action recognition under networking corruptions and clean data. Networking corruptions hurt model performance across benchmarks.

4 Impacts on Video ML Models

We assess the impact of networking corruptions on video ML models. We study models from four tasks: action recognition (Section 4.1), object tracking (Section 4.2), object segmentation (Section 4.3), and video captioning (Section 4.4). These tasks represent various prediction frequencies (one prediction per frame vs. one prediction per video) and modalities (i.e. segmentation mask vs. class prediction).

We summarize our main findings in Table 2. Networking corruptions impact performance on all tasks, but effects vary by task and dataset. Visual artifacts negatively affect most tasks. Intuitively, they can obscure objects in a video, destroying action or location information necessary for specific video tasks. Temporal truncation largely impacts tasks with one prediction per video. Datasets with shorter videos are more vulnerable: on HMDB51 (action recognition), even minor truncation may remove necessary action information. Datasets where temporal context is crucial, such as SSV2, are also especially impacted by temporal truncation. However, segmentation and tracking, which feature frame-by-frame outputs, are less affected, since making the correct prediction on a particular frame requires less temporal context.

Evaluation method We report standard performance metrics for each task. Since networking corruptions can cause videos to become unreadable, we report metrics over videos that remain readable after streaming through each link. For object tracking & segmentation, the original annotations may not be aligned with frames from corrupted videos. We align ground-truth annotations by matching them to the closest (mean-squared error) frame in the corrupted video. Full details are in Appendix A.

4.1 Action Recognition

On action recognition, visual artifacts impact all models and datasets, but temporal truncation impacts only certain datasets.

Datasets and models We evaluate accuracy for a 50-layer TSN [39] on HMDB51, UCF101, Kinetics-400, and SSV2. On Kinetics-400, we also evaluate TSM [27], 3D-ResNet [14], I3D [5], SlowFast [10] and IR-CSN [38]. On HMDB51, we also evaluate 3D-ResNet18.

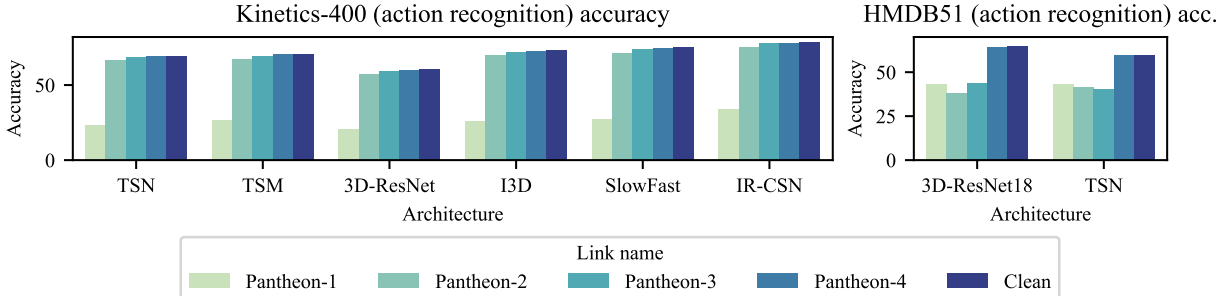


Figure 8: **Left:** (from left to right) Accuracy of TSN, TSM, 3D-ResNet, I3D, SlowFast, and IR-CSN on Pantheon-1 to -4 and clean data, Kinetics-400. **Right:** (from left to right) Accuracy of 3D-ResNet18 and TSN, on Pantheon-1 to -4 and clean data, HMDB51. Networking corruptions degrade performance across model architectures.

Visual artifacts lower performance across action recognition datasets and models Figure 7 compares performance on each dataset under networking corruptions. Figure 8 shows the performance of various models under networking corruptions. Over all models and datasets, Pantheon-1 (leftmost bar in each group) lowers accuracy up to 46.0% (Kinetics-400, 69.4% to 23.4%). Pantheon-2, -3, and -4 do not always lower performance. This suggests that visual artifacts—common in Pantheon-1—degrade action recognition performance.

We isolate the effect of visual artifacts by streaming HMDB51 at varying packet loss rates (correlated with visual artifacts). Figure 9 (top left) confirms that higher packet loss rate hurts accuracy. Thus, visual artifacts from packet loss explain some of the performance drop.¹

Temporal truncation hurts performance on certain datasets Figure 7 shows that Pantheon-2 and -3—which primarily cause temporal truncation—impact HMDB51 and SSV2 accuracy. These datasets may be vulnerable to truncation. HMDB51 has short videos (median: 2.67s)—even minor truncation significantly reduces the amount of signal for action recognition. SSV2 requires more temporal context (e.g. object moving to the left), so SSV2 is also more sensitive to truncation.

We isolate the impact of temporal truncation by varying video length and bandwidth limits on HMDB51. Figure 9 (top middle) shows that performance drops as video length decreases. In Figure 9 (top right), performance drops similarly as bandwidth limit decreases. This pinpoints how much of the performance drop is caused by temporal truncation.²

4.2 Object Tracking

In summary, object tracking is highly sensitive to visual artifacts, but not truncation.

¹We examined file checksums/out-of-distribution detection to filter examples with heavy artifacts, but did not use them for our main results as they often discarded clean videos (see Appendix C).

²Empirically, methods to lower bandwidth overhead (i.e. downsampling, switching codec) to mitigate truncation resulted in negative impacts/tradeoffs with ML performance (see Appendix C).

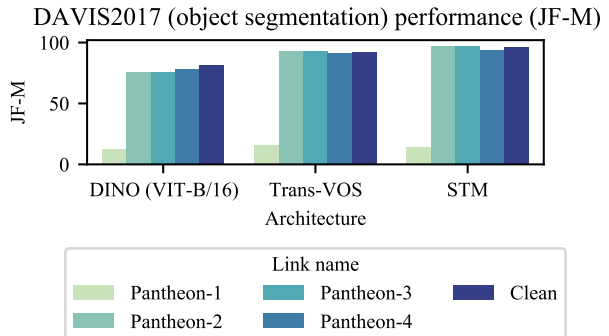


Figure 11: (from left to right) DINO, Trans-VOS, and STM performance, DAVIS2017, on Pantheon-1 to -4 and clean data. Pantheon-1 degrades performance (strong visual artifacts); other links do not.

Impact of network conditions/video parameters on video ML performance

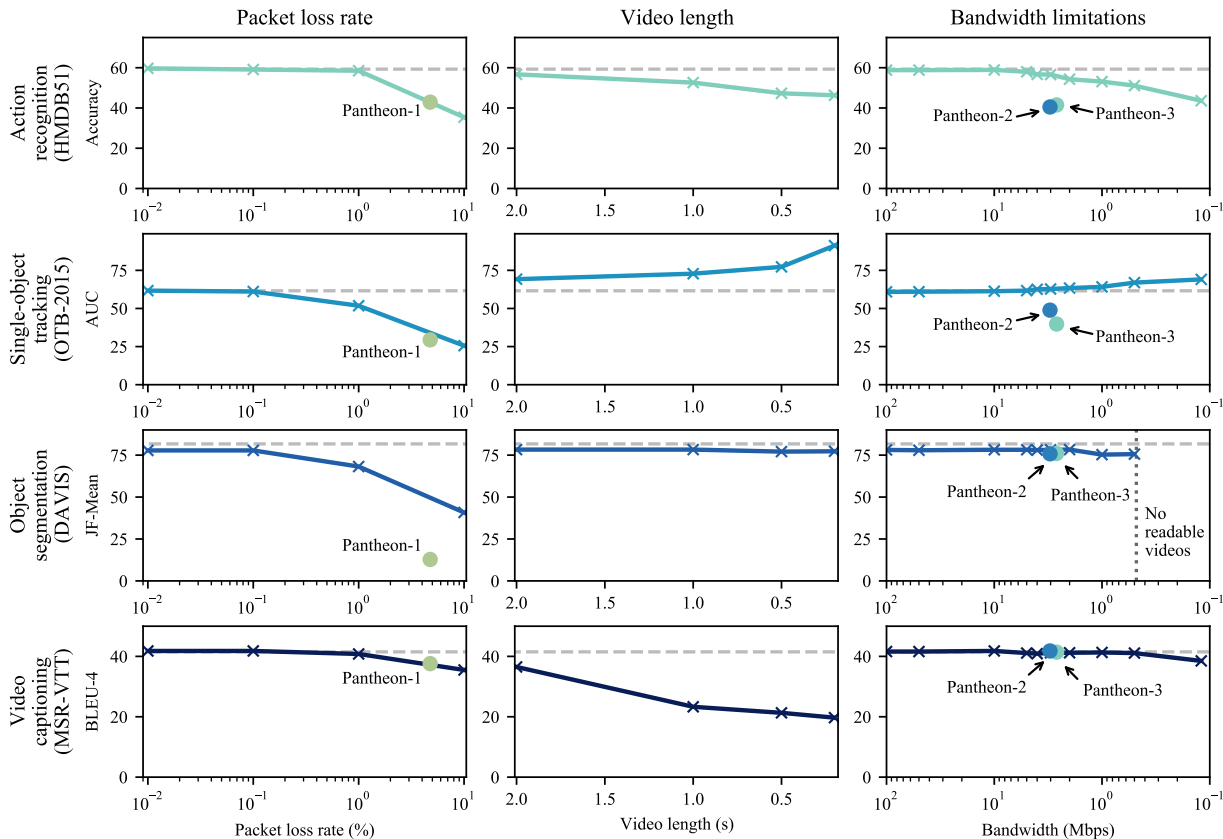


Figure 9: **Top:** TSN accuracy (HMDB51, action recognition) under varying packet loss rate (*left*), video length (*center*), and bandwidth (*right*). **2nd from top:** PrDIMP AUC (OTB-2015, single-object tracking) under varying packet loss rate (*left*), video length (*center*), and bandwidth (*right*). **3rd from top:** DINO JF-Mean (DAVIS, object segmentation) under varying packet loss rate (*left*), video length (*center*), and bandwidth (*right*). **Bottom:** UniVL BLEU-4 (MSR-VTT, video captioning) under packet loss rate (*left*), video length (*center*), and bandwidth (*right*).

Datasets and models We report AUC on OTB-2015 for four object trackers: SiamRPN [25], SiamFC++ [43], KYS [1], and PrDIMP [6].

Visual artifacts in Pantheon 1-3 degrade object tracking performance Figure 10 shows single-object tracking performance under networking corruptions.³ Networking corruptions on Pantheon-1 to -3 degrade performance, likely due to visual artifacts. Since objects must be tracked continuously, even small artifacts can disrupt tracking performance by obscuring object(s) of interest. As OTB-2015 has longer videos (median: $13.1s^4$), there is more time for visual artifacts to impact tracking. We confirm this by varying packet loss rate on OTB-2015: Figure 9 (2nd row, left) shows that tracking AUC drops as packet loss rate exceeds 0.1%.

Object tracking is relatively robust to temporal truncation Tracking may be easier on short videos, since visual artifacts have less time to disrupt tracking. In fact, temporal truncation can artificially inflate tracking performance. We confirm this by varying video length on OTB-2015. Figure 9 (2nd row, middle) shows that performance improves as video length decreases. As an

³Visual artifacts are prevalent on OTB-2015 (even on a clean link). Thus, our baseline is performance on videos streamed via a clean link.

⁴For datasets with only raw frames (DAVIS & OTB-2015), we compute video length assuming 30 FPS, a standard frame rate.

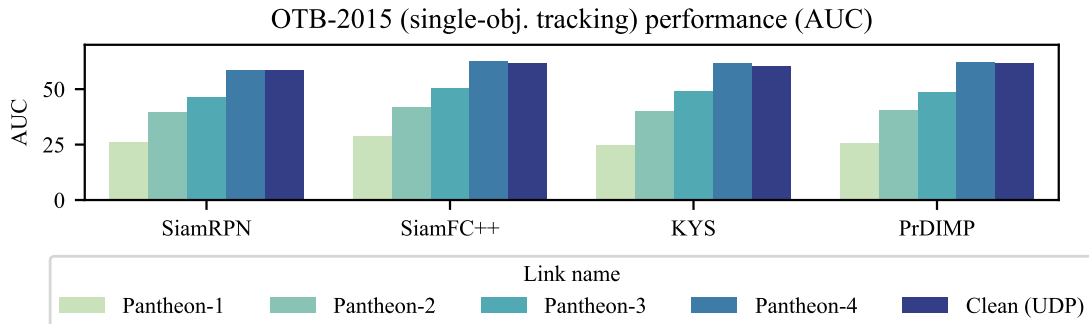


Figure 10: (from left to right) SiamRPN, SiamFC++, KYS, and PrDIMP performance, OTB-2015, on Pantheon-1 to -4 and a clean link. Networking corruptions hurt object tracking performance across multiple architectures and network links.

Table 3: MSR-VTT Captioning Performance Under Networking Corruptions

Link	BLEU-4	ROUGE-L	METEOR
Pantheon-1	37.6	57.8	26.3
Pantheon-2	41.4	60.3	28.1
Pantheon-3	41.8	60.4	28.3
Pantheon-4	41.4	60.8	28.8
Clean	41.5	60.9	29.0

extreme case, AUC improves by 29.6 when video length drops to 0.2s. AUC similarly improves as bandwidth decreases (Figure 9, 2nd row, right).

4.3 Video Object Segmentation

Video object segmentation models are susceptible to visual artifacts, but not temporal truncation—although our evaluation method may be overly lenient.

Datasets and Models We evaluate DINO [4], STM [30] and TransVOS [48] on DAVIS2017 using JF-mean score. JF-Mean averages the overlap between the predicted vs. ground-truth mask with mask boundary detection.

Visual artifacts impact video object segmentation Figure 11 shows that Pantheon-1 lowers JF-Mean on all methods up to 82.8 points (96.2 to 14.0, STM). Segmentation may be susceptible to visual artifacts: they can destroy object location information necessary for segmentation. We investigate this by varying packet loss levels. Figure 11 (third row, left) shows that increasing levels of packet loss negatively impacts performance, suggesting that visual artifacts contribute to the performance drop.

Truncation has little impact on object segmentation No major performance drops occur on other Pantheon links, or under varying video length and bandwidth (Figure 11, third row, middle and right). Our evaluation may be overly lenient: one clip remains readable on all links (“parkour”), so metrics are reported for that video. Also, Pantheon-2 and -3 truncate the “parkour” clip to ≤ 0.2 s. Thus, models only need to output high-quality masks for a few frames.

Table 4: Comparison of Generated Captions on MSR-VTT Under Various Networking Corruptions

Clean	Pantheon-1	Pantheon-2	Pantheon-3	Pantheon-4
a man is talking about a small egg	a man is talking about something	a man is talking about something	a man is talking about something	a man is talking about a product
a minecraft character is walking around	someone is playing a game	someone is playing a game	a minecraft character is walking around	a minecraft character is walking around
a man is standing on the stairs and talking	there is a man with cap is walking on the floor	a man is standing	a man is standing	a man is standing on the stairs and talking

4.4 Video Captioning

On video captioning models, networking corruptions slightly lower standard captioning metrics, but generated captions may change significantly.

Datasets and models We evaluate UniVL [28] on the MSR-VTT benchmark. We report three standard metrics for caption quality: BLEU-4, ROUGE-L, and METEOR. BLEU-4 is the proportion of 4-grams in the generated caption that appear in the reference caption. ROUGE-L rewards long common subsequences between generated and reference captions. METEOR is an F-measure of unigram precision and recall between generated and reference captions, with a penalty for out-of-order words. Each generated caption is compared to 20 reference captions, yielding 20 scores. We retain the highest score.

Visual artifacts slightly impact video captioning metrics Table 3 shows that standard captioning metrics drop slightly on Pantheon-1 (-3.9 BLEU-4, -3.2 ROUGE-L, -2.7 METEOR). Performance slightly drops for the other links. Intuitively, visual artifacts may increase captioning difficulty by obscuring objects or actions. We confirm this by varying the amount of packet loss on MSR-VTT. Figure 9 (bottom left) shows that BLEU-4 drops slightly as packet loss rate exceeds 1%.

Severe truncation lowers video captioning metrics Figure 9 (bottom middle) shows that temporal truncation hurts performance at video lengths under 2.0s. However, MSR-VTT videos are relatively long (Figure 6), so performance is stable across bandwidth ranges common in Pantheon (Figure 9, bottom right).

Captioning outputs worsen under video streaming Despite small drops in captioning metrics, captions may worsen under video streaming. Table 4 compares captions generated under networking corruptions to those generated on clean videos. We find two failure modes: (1) word or phrase-level substitutions (Table 4, 1st+3rd rows) and rephrases (Table 4, 2nd row). Although captions remain grammatical, these can change or contradict the clean-data caption. Up to 74.4% of captions change after streaming (Pantheon-1); even without corruptions, 48.6% of captions change. Thus, video captioning models may still be sensitive to video streaming.

5 A Baseline Defense

We investigate whether data augmentation can improve robustness to networking corruptions. Data augmentation, which aims to improve ML model performance under distribution shifts, has shown promise as a defense for other corruptions [8, 15]. We find that data augmentation does not recover performance under networking corruptions. It slightly mitigates severe visual artifacts (+3.0% lift), but has little effect on temporal truncation. We evaluate six additional defenses, such as changes to

model training/streaming setup and filtering corrupted videos, in Appendix C. These also do not fully restore performance. Targeting specific artifacts is a potential future direction for improving robustness to networking corruptions.

Setup We train a 3D-ResNet18 on the HMDB51 action recognition dataset. During training, each clean video has a 50% chance to be replaced with network-corrupted video.

Data augmentation does not improve performance; shows minor promise for severe visual artifacts In Figure 12 (top), we find that data augmentation does not improve accuracy under networking corruptions. On HMDB51, augmentation improves performance by up to 0.7% (Pantheon-2), and worsens performance by up to 3.4% (Pantheon-4). However, Figure 12 (bottom left) shows that data augmentation may slightly mitigate the impact of severe visual artifacts (packet loss > 10%). At 20% packet loss, data augmentation restores 3.0% accuracy, but this lift decreases as packet loss rate decreases.

Data augmentation cannot mitigate truncation Figure 12 (bottom right) shows that data augmentation lowers accuracy under truncation up to 3.7% (50 & 100Mbps). Intuitively, temporal truncation increases action recognition difficulty, as there is less signal to learn from. Furthermore, if truncation removes the underlying action from a video, the ground-truth labels become unreliable. As-is, data augmentation may have trouble adapting to temporal truncation.

6 Related Work

ML robustness to data corruptions Recent work establishes benchmarks for varying types of distribution shifts in image data [12, 16, 15, 23]. Our work introduces networking corruptions as an additional failure mode for ML robustness studies.

Networking corruptions & video Video corruptions have been studied in networking in the context of video streaming [11] or codec-level issues [2, 18]. Network and codec-based solutions to streaming failures are proposed in [9, 22]. We see our work as complementary, analyzing the impact of networking corruptions in an ML context.

Video transmission in ML systems Researchers have proposed live video transmission for ML video analytics due to the cost of video ML model training. Our work may be of interest to that community. Distream [46] uses inter-camera workload-balancing to distribute video processing across multiple nodes. Spatula [19] further exploits physical-location correlation of cameras within a cluster. Chameleon [20] adapts neural network configurations (i.e. frame rate, resolution) to network conditions.

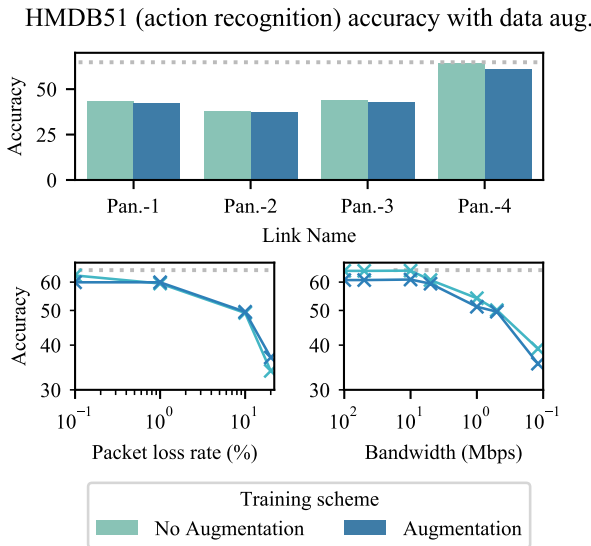


Figure 12: **Top:** Data augmentation performance using networking corruptions, HMDB51. **Bottom:** Data augmentation with varying packet loss rates (*left*) or bandwidth limitations (*right*). Data augmentation does not restore accuracy. It slightly mitigates impacts of high packet loss, but worsens performance at varying bandwidths.

7 Conclusion

We study the impact of networking corruptions on video ML. We discover networking corruptions in Kinetics-400. We then perform a simulation study, describing two artifact types that networking corruptions cause: visual artifacts and temporal truncation. These corruptions affect video ML models across four video tasks, but effects vary depending on how much temporal context is necessary. These variable effects reveal what information is important for various video tasks. Lastly, we find that data augmentation does not mitigate networking corruptions. We hope our work motivates further studies and defenses for networking corruptions.

Acknowledgments

We thank Simran Arora, Mayee Chen, Arjun Desai, Karan Goel, Sarah Hooper, Sharon Li, Laurel Orr, Eric Nguyen, Bibek Paudel, Christopher Ré, Nimit Sohoni, Sahaana Suri and Michael Zhang, for their helpful discussions and feedback on early drafts of the paper. We additionally thank Sadjad Fouladi for the helpful discussions, introducing us to the Mahimahi network simulator/Pantheon benchmark, and providing some computational resources; we also thank Du Tran for assistance with the CSN code repository. Furthermore, we would also like to acknowledge the FFmpeg community for assisting with patching the RTSP implementation. We gratefully acknowledge the support of the Department of Defense (DoD) through the National Defense Science and Engineering Graduate Fellowship (NDSEG) Program, the Dean’s Office of the Stanford School of Engineering through the Engineering Coterminal Fellowship Program, and members of the Stanford DAWN project: Facebook, Google, and VMWare.

References

- [1] Goutam Bhat, Martin Danelljan, Luc Van Gool, and Radu Timofte. Know your surroundings: Exploiting scene information for object tracking. In *Proceedings of the European Conference on Computer Vision*, 2020.
- [2] Fadi Boulos, Benoît Parrein, Patrick Le Callet, and David Hands. Perceptual effects of packet loss on H.264/AVC encoded videos. In *Fourth International Workshop on Video Processing and Quality Metrics for Consumer Electronics*, 2009.
- [3] Fabian Caba Heilbron, Victor Escorcia, Bernard Ghanem, and Juan Carlos Niebles. ActivityNet: A large-scale video benchmark for human activity understanding. In *IEEE/CVF Conference on Computer Vision and Pattern Recognition (CVPR)*, 2015.
- [4] Mathilde Caron, Hugo Touvron, Ishan Misra, Hervé Jégou, Julien Mairal, Piotr Bojanowski, and Armand Joulin. Emerging properties in self-supervised vision transformers. *arXiv:2104.14294*, 2021.
- [5] João Carreira and Andrew Zisserman. Quo vadis, action recognition? A new model and the Kinetics dataset. In *IEEE/CVF Conference on Computer Vision and Pattern Recognition (CVPR)*, 2017.
- [6] Martin Danelljan, Luc Van Gool, and Radu Timofte. Probabilistic regression for visual tracking. In *IEEE/CVF Conference on Computer Vision and Pattern Recognition (CVPR)*, 2020.

- [7] Jia Deng, Wei Dong, Richard Socher, Li-Jia Li, Kai Li, and Li Fei-Fei. Imagenet: A large-scale hierarchical image database. In *IEEE Conference on Computer Vision and Pattern Recognition (CVPR)*, 2009.
- [8] Samuel F. Dodge and Lina Karam. Understanding how image quality affects deep neural networks. *Eighth International Conference on Quality of Multimedia Experience (QoMEX)*, pages 1–6, 2016.
- [9] Nick Feamster and Hari Balakrishnan. Packet loss recovery for streaming video. In *12th International Packet Video Workshop*, 2002.
- [10] Christoph Feichtenhofer, Haoqi Fan, Jitendra Malik, and Kaiming He. SlowFast networks for video recognition. In *IEEE International Conference on Computer Vision (ICCV)*, 2019.
- [11] Jaroslav Frnda, Miroslav Voznak, and Lukas Sevcik. Impact of packet loss and delay variation on the quality of real-time video streaming. *Telecommunication Systems*, 62(2), 2016.
- [12] Robert Geirhos, Patricia Rubisch, Claudio Michaelis, Matthias Bethge, Felix A. Wichmann, and Wieland Brendel. ImageNet-trained CNNs are biased towards texture; increasing shape bias improves accuracy and robustness. In *7th International Conference on Learning Representations (ICLR)*, 2019.
- [13] Raghav Goyal, Samira Ebrahimi Kahou, Vincent Michalski, Joanna Materzynska, Susanne Westphal, Heuna Kim, Valentin Haenel, Ingo Fruend, Peter Yianilos, Moritz Mueller-Freitag, et al. The “something something” video database for learning and evaluating visual common sense. In *IEEE International Conference on Computer Vision (ICCV)*, 2017.
- [14] Kensho Hara, Hirokatsu Kataoka, and Yutaka Satoh. Can spatiotemporal 3D CNNs retrace the history of 2D CNNs and ImageNet? In *IEEE/CVF Conference on Computer Vision and Pattern Recognition (CVPR)*, 2018.
- [15] Dan Hendrycks, Steven Basart, Norman Mu, Saurav Kadavath, Frank Wang, Evan Dorundo, Rahul Desai, Tyler Zhu, Samyak Parajuli, Mike Guo, Dawn Song, Jacob Steinhardt, and Justin Gilmer. The many faces of robustness: A critical analysis of out-of-distribution generalization. In *IEEE International Conference on Computer Vision (ICCV)*, 2021.
- [16] Dan Hendrycks and Thomas G. Dietterich. Benchmarking neural network robustness to common corruptions and perturbations. In *International Conference on Learning Representations (ICLR)*, 2019.
- [17] Dan Hendrycks, Kevin Zhao, Steven Basart, Jacob Steinhardt, and Dawn Song. Natural adversarial examples. *arXiv:1907.07174*, 2019.
- [18] Arpad Huszák and Sandor Imre. Analysing GOP structure and packet loss effects on error propagation in MPEG-4 video streams. In *4th International Symposium on Communications, Control and Signal Processing (ISCCSP)*, 2010.
- [19] Samvit Jain, Xun Zhang, Yuhao Zhou, Ganesh Ananthanarayanan, Junchen Jiang, Yuanchao Shu, Victor Bahl, and Joseph Gonzalez. Spatula: Efficient cross-camera video analytics on large camera networks. In *ACM/IEEE Symposium on Edge Computing (SEC)*, 2020.

- [20] Junchen Jiang, Ganesh Ananthanarayanan, Peter Bodik, Siddhartha Sen, and Ion Stoica. Chameleon: Scalable adaptation of video analytics. In *Proceedings of the 2018 Conference of the ACM Special Interest Group on Data Communication*, 2018.
- [21] Will Kay, João Carreira, Karen Simonyan, Brian Zhang, Chloe Hillier, Sudheendra Vijayanarasimhan, Fabio Viola, Tim Green, Trevor Back, Paul Natsev, Mustafa Suleyman, and Andrew Zisserman. The Kinetics human action video dataset. *arXiv:1705.06950*, 2017.
- [22] Mohammad Kazemi, Razib Iqbal, and Shervin Shirmohammadi. Joint intra and multiple description coding for packet loss resilient video transmission. *IEEE Transactions on Multimedia*, 20(4), 2017.
- [23] Pang Wei Koh, Shiori Sagawa, Henrik Marklund, Sang Michael Xie, Marvin Zhang, Akshay Balsubramani, Weihua Hu, Michihiro Yasunaga, Richard Lanus Phillips, Irena Gao, Tony Lee, Etienne David, Ian Stavness, Wei Guo, Berton A. Earnshaw, Imran S. Haque, Sara Beery, Jure Leskovec, Anshul Kundaje, Emma Pierson, Sergey Levine, Chelsea Finn, and Percy Liang. WILDS: A benchmark of in-the-wild distribution shifts. In *International Conference on Machine Learning (ICML)*, 2021.
- [24] Hilde Kuehne, Hueihan Jhuang, Estibaliz Garrote, Tomaso Poggio, and Thomas Serre. HMDB: A large video database for human motion recognition. In *IEEE International Conference on Computer Vision (ICCV)*, 2011.
- [25] Bo Li, Junjie Yan, Wei Wu, Zheng Zhu, and Xiaolin Hu. High performance visual tracking with siamese region proposal network. In *IEEE/CVF Conference on Computer Vision and Pattern Recognition (CVPR)*, 2018.
- [26] Shiyu Liang, Yixuan Li, and R. Srikant. Enhancing the reliability of out-of-distribution image detection in neural networks. In *International Conference on Learning Representations (ICLR)*, 2018.
- [27] Ji Lin, Chuang Gan, and Song Han. Tsm: Temporal shift module for efficient video understanding. In *IEEE/CVF International Conference on Computer Vision (ICCV)*, 2019.
- [28] Huaishao Luo, Lei Ji, Botian Shi, Haoyang Huang, Nan Duan, Tianrui Li, Jason Li, Taroon Bharti, and Ming Zhou. UniVL: A unified video and language pre-training model for multimodal understanding and generation. *arXiv:2002.06353*, 2020.
- [29] Ravi Netravali, Anirudh Sivaraman, Somak Das, Ameesh Goyal, Keith Winstein, James Mickens, and Hari Balakrishnan. Mahimahi: Accurate record-and-replay for HTTP. In *USENIX Annual Technical Conference (USENIX ATC)*, 2015.
- [30] Seoung Wug Oh, Joon-Young Lee, Ning Xu, and Seon Joo Kim. Video object segmentation using space-time memory networks. *IEEE Transactions on Pattern Analysis and Machine Intelligence*, 2019.
- [31] Jordi Pont-Tuset, Federico Perazzi, Sergi Caelles, Pablo Arbeláez, Alex Sorkine-Hornung, and Luc Van Gool. The 2017 DAVIS challenge on video object segmentation. *arXiv:1704.00675*, 2017.
- [32] John Postel. User datagram protocol. RFC 768, RFC Editor, 1980.
- [33] Iain E. G. Richardson. *H.264 and MPEG-4 Video Compression*. Wiley, 2003.

- [34] H. Schulzrinne, A. Rao, R. Lanphier, M. Westerlund, and M. Stiemerling. Real-time streaming protocol version 2.0. RFC 7826, RFC Editor, 2016.
- [35] Karen Simonyan and Andrew Zisserman. Very deep convolutional networks for large-scale image recognition. In *International Conference on Learning Representations (ICLR)*, 2015.
- [36] Khurram Soomro, Amir Roshan Zamir, and Mubarak Shah. UCF101: A dataset of 101 human actions classes from videos in the wild. *arXiv:1212.0402*, 2012.
- [37] Thomas Stockhammer and Miska M. Hannuksela. H.264/AVC video for wireless transmission. *IEEE Wireless Communications*, 12(4), 2005.
- [38] Du Tran, Heng Wang, Matt Feiszli, and Lorenzo Torresani. Video classification with channel-separated convolutional networks. In *IEEE International Conference on Computer Vision (ICCV)*, 2019.
- [39] Limin Wang, Yuanjun Xiong, Zhe Wang, Yu Qiao, Dahua Lin, Xiaoou Tang, and Luc Van Gool. Temporal segment networks: Towards good practices for deep action recognition. In *European Conference on Computer Vision (ECCV)*. Springer, 2016.
- [40] Eric Wong, Leslie Rice, and J. Zico Kolter. Fast is better than free: Revisiting adversarial training. In *International Conference on Learning Representations (ICLR)*, 2020.
- [41] Yi Wu, Jongwoo Lim, and Ming-Hsuan Yang. Object tracking benchmark. *IEEE Transactions on Pattern Analysis and Machine Intelligence*, 37(9), 2015.
- [42] Jun Xu, Tao Mei, Ting Yao, and Yong Rui. Msr-vtt: A large video description dataset for bridging video and language. In *IEEE/CVF Conference on Computer Vision and Pattern Recognition (CVPR)*, 2016.
- [43] Yinda Xu, Zeyu Wang, Zuoxin Li, Ye Yuan, and Gang Yu. SiamFC++: Towards robust and accurate visual tracking with target estimation guidelines. In *Proceedings of the AAAI Conference on Artificial Intelligence*, 2020.
- [44] Francis Y. Yan, Jestin Ma, Greg D. Hill, Deepti Raghavan, Riad S. Wahby, Philip Levis, and Keith Winstein. Pantheon: the training ground for Internet congestion-control research. In *USENIX Annual Technical Conference (USENIX ATC)*, 2018.
- [45] Dahua Lin Yue Zhao, Yuanjun Xiong. MMAction. <https://github.com/open-mmlab/maction>, 2019.
- [46] Xiao Zeng, Biyi Fang, Haichen Shen, and Mi Zhang. Distream: Scaling live video analytics with workload-adaptive distributed edge intelligence. In *Proceedings of the 18th Conference on Embedded Networked Sensor Systems*, 2020.
- [47] Xiao Zeng, Ming Yan, and Mi Zhang. Mercury: A framework for efficient and elastic on-device distributed DNN training. In *ACM Conference on Embedded Networked Sensor Systems (SenSys)*, 2021.
- [48] Yizhuo Zhang, Zhirong Wu, Houwen Peng, and Stephen Lin. A transductive approach for video object segmentation. In *IEEE/CVF Conference on Computer Vision and Pattern Recognition (CVPR)*, 2020.

Lost in Transmission: The Impact of Networking Corruptions on Video Machine Learning Models (Supplementary Material)

We describe experimental setups in more detail and provide additional experimental results. In Appendix A, we describe the complete experimental setup for all experiments, including preprocessing and training details. In Appendix B, we provide complete results for all our experiments. In Appendix C, we discuss a selection of additional defenses against networking corruptions, but we do not find any to be fully successful.

A Experimental Details

Table 5: Pantheon Network Link Parameters Used for Simulation Study

Network link name	p	B (Mbps)	Time-Var.	t (ms)	S
Pantheon-1 (Nepal → AWS India, Wi-Fi)	4.77	0.57	Y	28	14
Pantheon-2 (Mexico → AWS California, Cellular)	0	2.64	Y	88	130
Pantheon-3 (AWS Brazil → Colombia, Cellular)	0	3.04	Y	130	426
Pantheon-4 (India → AWS India, Wired)	0	100.42	N	27	173
Pantheon-5 (AWS Korea → China, Wired)	0.06	77.72	N	51	94
Pantheon-6 (AWS California → Mexico, Wired)	0	114.68	N	45	450

A.1 Video Streaming Details

Streaming. Videos are streamed in real-time at their native frame rate using the `-re` flag, and encoded as an H.264 bitstream before transmission. For frame-based datasets, images are converted into a H.264-encoded MP4 video at 25 FPS prior to streaming, then converted back into JPEG images using the highest possible quality settings (`-qmin` and `-qmax` set to 1). Some videos become unreadable after streaming.

Link Parameters. We provide the precise settings for all 6 real-world Pantheon links in Table 5.¹ Empirically, we found that testing on Pantheon-1 through -4 was sufficient to demonstrate the variety of impacts that networking corruptions have on video ML models. Specifically, Pantheon-4, -5, and -6 usually had similar impacts on ML model performance. Although we explore the effects of the first four Pantheon links in the main paper, we provide results of our experiments over all six links here for completeness.

¹As reported at <https://pantheon.stanford.edu/measurements/emu/>.

A.2 Evaluation Setup

Preprocessing. We use RGB features only. Videos are channel-normalized under the same settings as training, namely, ActivityNet [3] normalization for 3D-ResNets and ImageNet [7] normalization for the remaining. Inputs are also scaled to the same spatial size used for training. Likewise, temporal clips are sampled under the same length and sampling rate used in training. For 3D-ResNets, this constitutes 112×112 pixel videos, while for the other architectures, we use short-edge scaling with short side length 224px, keeping the original aspect ratio. Temporally, we use 16 frame clips for 3D-ResNets, and 32 frame clips for the remaining architectures after temporal downsampling by a factor of 2 (i.e., every other frame). This serves to match the train-test distributions for these video models as closely as possible, thus isolating networking corruptions as the only distributional shift in our experiments.

Annotation alignment. Empirically, after streaming via UDP, video clips may have missing or duplicate frames² due to lost packets. As UDP does not guarantee the receipt of outgoing packets, any lost packets are recoverable. Thus, frame-level mismatches may cause off-by-N errors if corrupted videos are directly evaluated with the ground-truth annotations. As a concrete example, one might observe that the 3rd frame of a particular corrupted video is visually identical to the 5th frame of the corresponding clean video, the 4th corrupted frame resembles the 6th clean frame, and so on.³

To combat this, we perform an annotation alignment step, which matches ground-truth frames and their corresponding annotations to corrupted-video frames. For every frame, we search for the nearest frames in the clean video as measured by pixel-wise mean-squared error (MSE). As a further optimization, as only a few frames are usually dropped, we search only in the temporal neighborhood of the current frame by looking up to 10 frames forward from the last-matched frame in the clean video, and accepting a frame as a “match” if its difference falls under a certain MSE threshold. We use an MSE threshold of 100 for DAVIS and OTB-2015. When no match is found, we default to the closest MSE match in that window. We continue matching frames until all corrupt frames have a matching clean frame. Then, we assign as the annotation of the corrupt frame the corresponding annotation of the matched clean frame. Finally, we evaluate the corrupted video sequence using the corresponding annotations.

Evaluation Strategy. On action recognition, for fair comparison during inference, on 2D-backbone architectures, we sample eight frames and apply a ten-crop as in [39], and on 3D-backbone architectures, we sample 10 clips and apply a three-crop, following the setup of [45, 10], to emulate fully convolutional testing [35]. Pretrained model weights are sourced from MMAAction [45]⁴, except for two models: (1) 3D-ResNets, which are either sourced from the original paper authors’ code repository [14]⁵ or trained using the setup described below, and (2) CSN, which is sourced from the original authors’ code repository [38]⁶.

For DAVIS, we use the official evaluation repository. For OTB-2015, all repositories use equivalent evaluation procedures within each benchmark. For MSR-VTT, since we test one method in each of those tasks, we use the evaluation method of that repository.

Since videos can become readable during transmission, for comparability across all experiments, we report performance metrics over the subset of videos that remained readable on all six Pantheon links, or the *readable intersection*. For experiments that stream videos on other link settings, such as

²Lost information in non-keyframes destroys motion information, giving the video an illusion of “freezing” or duplicate frames.

³Illustrative example only. Actual alignments may vary.

⁴<https://github.com/open-mmlab/mmaaction2>

⁵<https://github.com/kenshohara/3D-ResNets-PyTorch>

⁶<https://github.com/facebookresearch/vmz>

the experiments on varying network parameters or alternative defenses for networking corruptions, we report performance over the same subset of videos. In experiments where a video from the *readable intersection* is missing, which can happen on experiments that vary networking parameters or the streaming setup, the model’s prediction on that video is marked as incorrect.

A.3 Training Setup

Action Recognition. We train 3D-ResNet18 on HMDB51 following the setup of [14]. For each video clip, we randomly select a contiguous 16-frame segment. Then, all images are first channel-normalized with respect to the ActivityNet [3] mean. Following normalization, we apply a multiscale random crop with aspect ratio one at scales $\{1, 1/2^{1/4}, 1/\sqrt{2}, 1/2^{3/4}, 1/2\}$, choosing one of the four corners + center of the video to crop (as in a five-crop). We then resize all videos to have size 112×112 pixels. We then train for 50 epochs using a starting learning rate of 0.001 with weight decay 10^{-5} , optimizing using stochastic gradient descent. When validation loss saturates for 10 epochs, we decrease learning rate by a factor of 10. For more details, consult the method of [14].

Video Captioning. We train the video captioning model following the setup of UniVL [28], as well as their method for video feature extraction.⁷

A.4 Ablation Setup

For each ablation experiment, we select a particular value for either packet loss rate, video length, or bandwidth limitations, and stream videos across an otherwise clean link. For Kinetics-400 and SSV2, due to the size of the datasets and computational cost of simulating networking corruptions, we conduct our ablation study on samples of 2000 and 1000 videos, denoted Kinetics-Mini and SSV2-Mini, respectively.

Packet loss rate. Ablations on packet loss rate allow us to isolate the impact of visual artifacts. We measure performance on videos subjected to packet loss rates of 0.01%, 0.1%, 1%, 10%, and 20%.

Video length. Manual control over video length allows us to stratify by the severity of temporal truncation. We examine performance on videos where only the first 0.2s, 0.5s, 1s, and 2s is streamed.

Bandwidth limitations. Adjusting bandwidth limitations on links allows us to isolate the impact of temporal truncation. We measure performance on videos streamed with bandwidth limitations of 0.12, 0.5, 1, 2, 3, 4, 5, 10, 50, and 100 Mbps.

A.5 Other

Software. All development is done on Python using PyTorch 1.7 with Torchvision 0.8.1. Network simulation is done using Mahimahi [29] with the UDP [32] protocol. We use a branch of FFmpeg 4.2 for point-to-point RTSP [34] based streaming, with an additional patch to the RTSP streaming implementation.

Hardware. We use a single V100 GPU for model training and evaluation. Simulating network corruptions can be done on CPU only, though for speed, we used 16-core processors (i.e., an AWS c5.4xlarge) since the simulations are highly parallelizable.

Sourcing models. We source models from the official code release for the paper when possible, except for action recognition tasks, for which we source models from MMAAction [45] and the Facebook Video Model Zoo [38] (CSN only).

⁷<https://github.com/ArrowLuo/VideoFeatureExtractor>

Table 6: Action Recognition Accuracies by Pantheon Link, Kinetics-400

Link	TSN	TSM	3D-ResNet	I3D	SlowFast	IR-CSN
Kinetics-Pantheon-1	23.4	26.3	20.3	25.7	27.3	33.6
Kinetics-Pantheon-2	66.6	67.0	57.3	69.8	71.4	75.4
Kinetics-Pantheon-3	68.6	69.4	59.4	71.9	74.1	77.5
Kinetics-Pantheon-4	69.4	70.2	59.9	72.8	74.6	78.0
Kinetics-Pantheon-5	68.6	69.5	59.1	72.1	73.9	77.6
Kinetics-Pantheon-6	69.3	70.0	60.0	72.7	74.2	77.9
Clean	69.4	70.4	60.0	72.9	75.0	78.4

Table 7: Action Recognition Accuracies by Pantheon Link, HMDB51

Link	3D-ResNet18	TSN
HMDB-Pantheon-1	43.3	42.9
HMDB-Pantheon-2	37.7	41.5
HMDB-Pantheon-3	4	40.5
HMDB-Pantheon-4	64.2	59.6
HMDB-Pantheon-5	64.5	58.6
HMDB-Pantheon-6	64.6	59.7
Clean	64.8	59.3

B Full Experimental Results

In this section, we provide full results for our study on the impact of networking corruptions on video ML models. We include an architectural study, and ablations on packet loss, video length, and bandwidth limitations for all tasks: action recognition (Appendix B.1), object tracking (Appendix B.2), object segmentation (Appendix B.3), and captioning (Appendix B.4). For action recognition, we additionally include a brief study on the impact of model capacity, finding that it does not improve robustness to networking corruptions. Finally, we discuss additional ablations over network parameters (Appendix B.5) and provide full statistics for how bandwidth limitations affect video length (Appendix B.6).

Table 8: Action Recognition Accuracies by Pantheon Link, UCF101

Link	3D-ResNet18	TSN
UCF-Pantheon-1	77.9	6
UCF-Pantheon-2	82.9	76.6
UCF-Pantheon-3	82.8	77.3
UCF-Pantheon-4	86.9	80.4
UCF-Pantheon-5	86.9	79.9
UCF-Pantheon-6	86.9	80.4
Clean	87.0	80.3

Table 9: Action Recognition Accuracies by Pantheon Link, SSV2

	TSN	TSM
SSV2-Pantheon-1	9.7	6.5
SSV2-Pantheon-2	21.0	26.5
SSV2-Pantheon-3	18.1	14.6
SSV2-Pantheon-4	33.4	57.5
SSV2-Pantheon-5	33.3	57.4
SSV2-Pantheon-6	33.4	57.5
Clean	34.4	57.0

Table 10: 3D-ResNet Accuracy on Clean and Corrupted Videos by Architecture Depth (d), Kinetics-400

Link	$d = 18$	$d = 34$	$d = 50$	$d = 101$
Kinetics-Pantheon-1	17.4	20.5	20.3	20.1
Kinetics-Pantheon-2	51.2	57.1	57.3	58.2
Kinetics-Pantheon-3	53.1	59.4	59.4	60.5
Kinetics-Pantheon-4	53.4	59.7	59.9	61.2
Kinetics-Pantheon-5	52.7	59.1	59.1	60.5
Kinetics-Pantheon-6	53.6	59.2	60.0	61.3
Kinetics-Clean	53.5	59.2	59.9	61.2

B.1 Full Results on Action Recognition

Architectural Study. We provide full results for our architectural study on Kinetics-400 in Table 6, HMDB51 in Table 7, UCF101 in Table 8, and SSV2 in Table 9. For action recognition, we evaluate 2D-backbone architectures like TSN [39] and TSM [27], and 3D-backbone architectures like 3D-ResNets [14], I3D [5], SlowFast [10], CSN [38], all with 50 layers.

Model Capacity. We provide full results for our study on the effect of model capacity in Table 10 as reported in Section 4.1, including results on Pantheon-5 and -6. Again, networking corruptions cause similarly-sized across model sizes, with slightly worse effects on larger-capacity models: on Pantheon-1, performance drops by 36.1% (3D-ResNet18) to 41.1% (3D-ResNet101).

Impact of packet loss. We perform our ablation study on the impact of packet loss on action recognition performance on TSN. Table 11 shows that packet loss adversely impacts model

Table 11: TSN Accuracy by Packet Loss Rate on HMDB51, UCF101, Kinetics-400, and SSV2

Packet loss rate (%)	HMDB51	UCF101	Kinetics-Mini	SSV2-Mini
0.01	59.7	80.4	67.4	33.0
0.1	59.1	79.9	66.8	33.2
1	58.5	77.1	60.4	31.3
10	35.4	50.7	24.5	20.0
20	24.6	32.0	12.5	11.2
Clean	59.3	80.3	69.4	34.4

Table 12: TSN Accuracy by Video Length (s) on HMDB51, UCF101, Kinetics-Mini, and SSV2-Mini

Length (s)	HMDB51	UCF101	Kinetics-Mini	SSV2-Mini
0.2	46.3	74.3	55.0	11.8
0.5	47.3	75.1	56.5	17.4
1	52.6	76.1	57.1	23.6
2	56.7	78.3	58.7	33.4
Clean	59.3	80.3	67.2	35.5

Table 13: TSN Accuracy by Bandwidth on HMDB51, UCF101, Kinetics-Mini, and SSV2-Mini

Bandwidth (Mbps)	HMDB51	UCF101	Kinetics-Mini	SSV2-Mini
0.12	43.6	75.2	57.6	8.5
0.5	51.1	78.1	61.6	12.8
1	53.1	78.5	63.6	13.6
2	54.3	79.2	65.2	16.6
3	56.6	79.2	64.7	21.9
4	56.7	79.3	6	25.6
5	58.0	79.2	63.5	27.8
10	58.9	80.0	66.9	32.7
50	58.8	80.3	67.4	32.9
100	58.8	80.3	67.2	32.9
Clean	59.3	80.3	67.2	35.5

performance across all datasets. Performance consistently drops as packet loss rate increases. Intuitively, as visual artifacts tend to worsen with increasing packet loss rate, sufficiently high levels of packet loss may destroy visual information necessary for classification.

Impact of video length. We study the impact of video length on action recognition using TSN as well. Table 12 shows that video truncation to fixed lengths hurts model performance across all datasets. Performance drops as truncation worsens. This result makes intuitive sense: more severe truncation means that more action information necessary for classification may be missing. Interestingly, UCF101 maintains high performance even under truncation.

Impact of bandwidth limitations. Again, we perform our ablation study on the impact of bandwidth limitations on action recognition performance on TSN. Table 13 shows that bandwidth limitations can hurt model performance across all datasets. Performance worsens as bandwidth limitations decrease further. However, datasets with shorter videos, such as HMDB51 and SSV2-Mini, which suffer up to a 24.4% accuracy drop (SSV2, 0.12Mbps) are much more severely impacted than datasets with longer videos, such as Kinetics-Mini and UCF101, which only suffer up to a 9.6% drop (Kinetics-Mini, 0.12Mbps). Intuitively, temporal truncation will disproportionately impact datasets with shorter videos: in shorter videos, truncation is more likely to destroy or cut into action information necessary for identifying an action.

B.2 Full Results on Video Object Tracking

Architectural study. We present the full results of our architectural study on video objecting in the OTB2015 single-object tracking benchmark in Table 14. For single-object tracking, we evaluate SiamRPN [25], SiamFC++ [43], KYS [1], and PrDIMP [6]. Because of the unusually high number

Table 14: Object Tracking Performance (AUC) by Pantheon Link, OTB-2015

Link	SiamRPN	SiamFC++	KYS	PrDIMP
OTB2015-Pantheon-1	25.9	28.8	24.4	25.6
OTB2015-Pantheon-2	39.6	41.5	39.8	40.5
OTB2015-Pantheon-3	46.4	50.3	48.9	48.5
OTB2015-Pantheon-4	58.3	62.3	61.5	62.0
OTB2015-Pantheon-5	57.6	60.2	60.0	61.0
OTB2015-Pantheon-6	57.7	61.5	60.9	61.1
Clean-UDP	58.3	61.9	60.8	61.6
Clean	64.8	68.4	69.5	70.5

Table 15: PrDIMP AUC by Packet Loss Rate, OTB-2015

Packet loss rate (%)	PrDIMP
0.01	61.7
0.1	61.0
1	51.8
10	25.6
20	16.4
Clean-UDP	61.6
Clean	70.5

of visual artifacts attributable to the usage of UDP, we report performance for data streamed on a clean link with UDP (Clean-UDP) as well.

Impact of packet loss. We evaluate the impact of packet loss rate on object tracking performance using PrDIMP for single-object tracking. Table 15 shows that increasing packet loss hurts tracking performance. Intuitively, visual artifacts, which emerge in the presence of packet loss, can disrupt tracking performance by destroying information about object location and shape across multiple frames.

Impact of video length. We quantify the effects of video length on object tracking performance, again using PrDIMP. Table 16 shows that as video length decreases, single-object tracking performance actually increases. As intuition, shorter videos are easier examples for object tracking, because objects in such clips only need to be tracked successfully for fewer frames. The longer the video, the more likely that subtle visual artifacts will disrupt tracking performance. As previously discussed, OTB-2015 is composed of relatively longer videos (median length 13.1s), exacerbating this issue.

Impact of bandwidth limitations. We study the effects of bandwidth limits on object tracking performance on PrDIMP. Table 17 shows that as the bandwidth limit decreases, object tracking performance improves. This is likely since decreasing bandwidth is correlated with shorter videos. This result is consistent with our ablation on video length.

B.3 Full Results on Video Object Segmentation

Architectural study. We present the full results for our architectural study on the DAVIS2017 video object segmentation benchmark in Table 18. For segmentation, we evaluate DINO [4], STM [30], and Trans-VOS [48]. For DINO in particular, we use the base vision transformer setting

Table 16: PrDIMP AUC by Video Length (s), OTB-2015

Length (s)	PrDIMP
0.2	91.3
0.5	78.5
1	75.7
2	72.4
Clean-UDP	61.6
Clean	70.5

Table 17: PrDIMP AUC by Bandwidth, OTB-2015

Bandwidth (Mbps)	PrDIMP
0.12	69.1
0.5	67.0
1	64.2
2	63.4
3	62.8
4	62.6
5	61.7
10	61.3
50	61.0
100	60.9
Clean-UDP	61.6
Clean	70.5

Table 18: Segmentation Performance by Pantheon Link, DAVIS

Link	DINO	STM	TransVOS
DAVIS-Pantheon-1	12.8	14.0	16.1
DAVIS-Pantheon-2	76.0	97.1	92.6
DAVIS-Pantheon-3	75.8	97.1	92.6
DAVIS-Pantheon-4	77.8	94.1	91.7
DAVIS-Pantheon-5	73.1	88.4	82.2
DAVIS-Pantheon-6	77.8	94.1	91.7
Clean	81.7	96.3	92.3

Table 19: DINO JF-Mean by Packet Loss Rate, DAVIS

Packet loss rate (%)	DINO
0.01	77.8
0.1	77.8
1	68.2
10	40.8
20	7.1
Clean	81.7

Table 20: DINO JF-Mean by Video Length (s), DAVIS

Length (s)	DINO
0.2	77.3
0.5	77.1
1	78.3
2	78.3
Clean	81.7

Table 21: DINO JF-Mean by Bandwidth, DAVIS

Bandwidth (Mbps)	DINO
0.12	N/A
0.5	75.6
1	75.3
2	78.3
3	78.2
4	78.2
5	78.2
10	77.2
50	77.9
100	78.1
Clean	81.7

(ViT-B/16) with patch size 16 due to memory constraints.

Impact of packet loss. We study the impact of packet loss on object segmentation on DAVIS using the DINO architecture. Table 19 shows that increasing packet loss consistently hurts model performance in terms of JF-Mean score. Intuitively, visual artifacts make it more difficult to output a correct segmentation mask, as the artifacts destroy information about object location and boundaries.

Impact of video length. We study the impact of video length on object segmentation on DAVIS using the DINO architecture. Table 20 shows that constricting video length slightly decreases segmentation performance up to 4.4 JF-Mean points. Intuitively, since segmentation mask predictions depend only on the current and previous frames, temporal truncation is unlikely to affect performance significantly.

Impact of bandwidth limitations. We study the impact of bandwidth limitations on object segmentation on DAVIS using the DINO architecture. We report results with the caveat that at 0.12Mbps, the set of readable videos was completely disjoint from the intersection of readable videos under Pantheon streaming. We denote this situation with the annotation “N/A.” Table 21 shows that as the bandwidth limit decreases, performance fluctuates, decreasing up to 6.1 JF-Mean points. This result is consistent with the ablation on video length. Ultimately, temporal truncation is unlikely to impact segmentation performance severely.

B.4 Full Results on Video Captioning

Architectural study. We present full results for video captioning on the MSR-VTT benchmark in Table 22. We evaluate UniVL under the video-only setup as described in [28].

Table 22: UniVL Captioning Performance by Pantheon Link, MSR-VTT

Link	BLEU-4	ROUGE-L	METEOR
MSR-VTT-Pantheon-1	37.6	57.8	26.3
MSR-VTT-Pantheon-2	41.4	60.3	28.1
MSR-VTT-Pantheon-3	41.8	60.4	28.3
MSR-VTT-Pantheon-4	41.4	60.8	28.8
MSR-VTT-Pantheon-5	41.3	60.7	28.8
MSR-VTT-Pantheon-6	41.5	60.8	28.8
Clean	41.5	60.9	29.0

Table 23: UniVL Captioning Performance by Packet Loss Rate, MSR-VTT

Packet loss rate (%)	BLEU-4	ROUGE-L	METEOR
0.01	41.8	60.7	28.5
0.1	41.8	60.8	28.6
1	40.8	60.2	28.2
10	35.5	56.6	25.3
20	30.0	52.8	22.8
Clean	41.5	60.9	29.0

Impact of packet loss. We isolate the impact of packet loss on video captioning performance. Interestingly, as shown in Table 23, packet loss does not severely impact captioning performance until packet loss rates exceed 10%. At high levels of packet loss, performance in terms of BLEU-4, ROUGE-L, and METEOR drops (-10.5 BLEU-4, -8.1 ROUGE-L, -6.1 METEOR at 20% packet loss rate). The performance drop makes intuitive sense: sufficient visual artifacts in corrupted video may destroy information relevant to the caption.

Impact of video length. We evaluate the impact of video length on video captioning performance. Table 24 shows that as video length decreases beyond 2s, captioning performance worsens. In fact, when truncated to 2s, captioning performance is already slightly degraded (-4.9 BLEU-4, -4.5 ROUGE-L, -3.8 METEOR). However, performance worsens as video length decreases: at 0.2s, performance drops by 21.8 BLEU-4, 12.6 ROUGE-L, and 9.2 METEOR points. The negative impact of truncation on video captioning makes intuitive sense: if truncation erases parts of the video with important objects or actions in the scene, the captioning task becomes more difficult, or even impractical.

Impact of bandwidth limitations. We evaluate the impact of bandwidth limits on video captioning performance. Table 25 shows that at bandwidth limits tested, video captioning performance drops trivially, with 0.12Mbps resulting in the worst performance drop (-2.9 BLEU-4, -2.7 ROUGE-L, -2.6 METEOR). This suggests that at the bandwidth limits in our ablation study, the temporal truncation is insufficient to adversely impact performance. This is expected as MSR-VTT features relatively long videos (median length 13.04s).

B.5 Additional Network Parameter Ablations

We briefly explore the effect of other network conditions on action recognition performance on HMDB51, namely time-varying packet arrivals, delay, and drop-tail queue size. We do not find that

Table 24: UniVL Captioning Performance by Video Length (s), MSR-VTT

Length (s)	BLEU-4	ROUGE-L	METEOR
0.2	19.7	48.3	19.7
0.5	21.3	50.8	21.2
1	23.3	53.9	23.3
2	36.5	56.4	25.1
Clean	41.5	60.9	29.0

Table 25: UniVL Captioning Performance by Bandwidth, MSR-VTT

Bandwidth (Mbps)	BLEU-4	ROUGE-L	METEOR
0.12	38.5	58.2	26.3
0.5	41.1	60.2	28.1
1	41.3	60.4	28.2
2	41.2	60.4	28.1
3	41.2	60.4	28.1
4	40.9	60.2	28.0
5	41.1	60.2	28.0
10	41.8	60.8	28.3
50	41.6	60.8	28.4
100	41.6	60.7	28.4
Clean	41.5	60.9	29.0

these settings non-trivially impact model performance.

Time-varying packet arrivals. Note that time-varying packet arrivals are used in Pantheon-1, -2, -3, the links that yielded the lowest downstream performance after streaming. We study the impact of time-varying links on Pantheon-1, -2, and -3 in isolation, replacing time-varying packet traces used for Pantheon-1, -2, and -3 with time-invariant packet traces of the same bandwidth, before streaming videos from the Kinetics-400 validation split through these links. Ultimately, this has little effect on model performance: our findings are that time-varying packet arrivals do not seem to affect accuracy in excess of 1.8% (Table 26). Neither does this choice of network parameter appear to have consistent effects on model performance: time-varying packet arrivals slightly improve accuracy on Pantheon-2 and -3 but slightly hurt accuracy on Pantheon-1. The

Table 26: 3D-ResNet50 Accuracy by Usage of Time-Varying Packet Arrivals, Kinetics-400

Link	Time-Var.?	Acc.
Pantheon-1	Y	58.1
	N	58.3
Pantheon-2	Y	59.4
	N	59.9
Pantheon-3	Y	59.7
	N	59.3
Clean	N/A	59.9

Table 27: 3D-ResNet18 Accuracy by Network Delay (ms), HMDB51

Delay	Acc.
100	55.5
50	58.8
10	61.5
No delay	64.8

Table 28: 3D-ResNet18 Accuracy by Queue Size (# of Packets), HMDB51

Queue Size	Acc.
1	4.8
5	46.4
10	60.0
50	62.4
100	63.0
500	62.9
Unlimited	64.8

effect is small and does not explain the accuracy drops seen for Pantheon-1, -2, -3 in the main paper.

Network Delay. Table 27 shows that increasing network delay appears to have a small but non-negligible effect on downstream model performance. On HMDB51, delays of 100ms resulted in a 9.3% accuracy drop. At 10ms of delay, however, the accuracy drop was much smaller (3.3% drop at 10ms delay). While we see higher delay levels on Pantheon-2, -3 (88ms, 130ms), our earlier analysis links the main mechanism of the accuracy drop to low bandwidth, not delay. Ultimately, the correlation between network delay and model performance is unclear, so our analysis is inconclusive.

Network uplink queue size. To understand the effect of queue size on model robustness, we evaluate the performance of 3D-ResNet18 on HMDB51 streamed with varying queue sizes. In the real-time video streaming setting, this queue contains network packets that have yet to be decoded from bit-space into pixel-space. We use a droptail queue for these experiments, meaning that arriving packets will be dropped if the queue is already full. Table 28 shows that droptail queue sizes larger than 10 packets have a small effect on model performance, with a 4.8% decline. However, at queue sizes of 1 and 5 packets, accuracy drops by 16.5% and 58.1%, respectively. Note that these two cases represent pathologically small droptail queue sizes, as all Pantheon links have queue sizes of at least 14 (Pantheon-1)

B.6 Video Length Statistics

We enumerate the median lengths for all videos streamed via Pantheon. Table 29 shows that as bandwidth limits decrease, video length decreases as well. Since the live-streaming process can change the average frame rate of a video, all lengths are renormalized based on the original frame rate of each video before streaming (length = # of frames / original frame rate). The number of frames is estimated using FFMpeg.⁸

⁸Frame counts on near-clean links may appear to slightly exceed original video length. This is because FFMpeg 4.2 sometimes overcounts the number of frames on the corrupted videos by one, which we found by manually counting frames for a small sample of streamed clips. Since SSV2 has an original frame rate of 12, this accounts for the 0.08s (1/12s) increase in video length over the original (Table 29). Similarly, HMDB51 has an original frame rate of 30,

Table 29: Median Video Length (s) by Bandwidth Limit, All Datasets

Dataset	Bandwidth (Mbps)										Orig.
	0.12	0.5	1	2	3	4	5	10	50	100	
HMDB51	0.07	0.43	0.60	0.77	0.93	1.17	1.50	2.50	2.63	2.63	2.67
UCF101	1.16	4.04	4.40	4.56	4.76	4.91	5.08	5.71	6.24	6.20	6.24
Kinetics-Mini	1.47	3.03	5.50	6.98	7.13	7.21	7.40	8.98	10.00	10.00	10.00
SSV2-Mini	0.08	0.33	0.33	0.83	1.33	1.83	2.25	3.75	4.25	4.25	4.17
OTB-2015	1.50	6.78	9.72	11.22	11.46	11.47	11.53	11.85	12.38	12.38	13.06
DAVIS	0.03	0.03	0.03	0.30	0.43	0.33	0.57	0.82	1.40	1.38	2.25
MSR-VTT	3.84	10.72	10.97	11.14	11.26	11.40	11.52	11.85	12.54	13.00	13.04

Table 30: Median Video Length (s) by Pantheon Link, All Datasets

Dataset	Link						Original
	Pan.-1	Pan.-2	Pan.-3	Pan.-4	Pan.-5	Pan.-6	
HMDB51	0.60	0.03	1.38	2.70	2.70	2.70	2.67
UCF101	3.88	4.84	4.76	6.20	6.20	6.24	6.24
Kinetics-Mini	5.84	8.44	8.51	10.00	9.54	10.00	10.00
SSV2-Mini	0.08	1.58	0.42	3.33	3.33	3.33	4.17
OTB-2015	11.16	11.43	11.16	12.43	12.38	12.47	13.06
DAVIS	0.60	0.05	0.17	1.40	1.48	1.40	2.25
MSR-VTT	10.28	11.31	11.28	13.01	13.01	13.01	13.04

Table 29 shows that as bandwidth limits decrease, video length decreases as well for all datasets. Note that bandwidth limits affect each dataset differently: some datasets suffer from truncation even at 100Mbps, while other datasets suffer no truncation. However, all datasets experience temporal truncation when the bandwidth limit is sufficiently small. Table 30 shows that most links cause some temporal truncation, but Pantheon-1 through -3 have disproportionate impacts on video length. These findings are consistent with our main study.

C Additional Defenses for Networking Corruptions

In addition to data augmentation, we evaluate the following methods as potential defenses against networking corruptions: (1) file checksums, (2) streaming with downsampled video, (3) usage of the HEVC video codec, (4) adversarial training, (5) decreasing training window size, (6) out-of-distribution filtering after streaming, and (7) network corruption-based data augmentation. For defenses involving training a model (adversarial training, decreasing training window size, and data augmentation), if not specified, all training details are the same as those described in Appendix A. No defense is able to fully restore performance, again reinforcing the need for targeted defenses for the specific artifacts and model failure modes that networking corruptions induce.

C.1 Methods

Checksums. We evaluate whether file checksums can be used as a filter for corrupted videos prior to inference. The intuition is that networking corruptions change the underlying bit-representation

which accounts for the 0.03s (1/30s) increase as well (Table 30).

of each video, suggesting the usage of file checksums to identify corrupted videos. We use the `md5sum` Linux utility to perform file-integrity checking.

Streaming with downsampled video. The intuition for downsampling during streaming is that this decreases the bandwidth requirement for streaming videos, potentially mitigating the impact of temporal truncation. Prior to the streaming process, we use the FFMpeg `scale` filter to downsize the video to 144p, 120p and 96p. We then train a model on clean videos at each resolution, and evaluate on networking-corrupted data with the same resolution.

HEVC codec. In contrast to the H.264 codec, the HEVC/H.265 codec achieves a better compression ratio, decreasing the bandwidth required for streaming videos. Intuitively, this can potentially mitigate the impact of temporal truncation. Concretely, we simply change the codec used during video transmission to the HEVC/H.265 codec.

Adversarial training. Adversarial training can potentially mitigate the impact of networking corruptions by limiting worst-case performance within a well-defined set of video perturbations. We augment our training data via the one-step ℓ_∞ -norm based fast gradient sign method (FGSM) attack [40]. We apply this adversarial perturbation to each video with probability 0.5.

Decreased training window size. Many video classification training methods, including the training scheme for 3D-ResNet, sample a fixed-size clip from each video for model training. We experiment with decreasing the window size from 16 frames to 8 and 4 frames during model training, with the idea that this can improve robustness to temporal truncation.

Out of distribution filtering. We use the ODIN out-of-distribution (OOD) detection method [26], which uses a threshold based on transformed softmax score for filtering OOD examples. Concretely, this is done using softmax with temperature, which can be computed for each example \mathbf{x}_i as follows:

$$S_i(\mathbf{x}) = \frac{\exp(f(x; \theta)/T)}{\sum_{i=1}^C \exp(f(x; \theta)/T)}, \quad (1)$$

where T is the temperature hyperparameter, C is the number of classes, and $f(x; \theta)$ is the model’s output. We then select a preset percentile α of the transformed maximum softmax score distribution on the in-distribution data to use as a threshold. During inference, the transformed maximum softmax score is compared to this threshold. Examples with transformed score below this threshold are marked as out-of-distribution and discarded. In our experiments, we choose $T = 1000$, $\alpha = 0.05$. We use HMDB validation split 2 to choose a threshold.

We report accuracy solely over the remaining examples. Furthermore, we also report the AUROC, treating ODIN as a pseudo-classifier for in- vs. out-of-distribution examples. Concretely, AUROC corresponds to the probability that a randomly selected clean example has a higher maximum softmax score than a randomly selected corrupted example.

Network Corruption-Based Data Augmentation. Intuitively, adding noise to the training data resembling networking corruptions may improve model robustness to networking corruptions, as augmentation yields a training distribution closer to the corrupted distribution. We augment the training data by replacing clean videos with their corrupted counterpart with probability 0.5. We train on videos perturbed on one particular link, and evaluate the performance of the resulting model on the validation set corrupted by the same link. Intuitively, this scheme leverages prior knowledge of exact network conditions to simulate networking corruptions that a model may encounter, conditioned on a pre-existing network link. We also attempted to augment training data using networking-corrupted videos from *all* links, but found in practice that this yielded worse performance on both clean data and networking-corrupted videos from individual links.

To better understand how data augmentation interacts with the artifacts seen under networking corruptions, we also evaluate packet-loss and bandwidth-constraint based augmentation. This allows

Table 31: Number of Videos with Matching/Non-Matching/Missing Checksums, HMDB51, UCF101, Kinetics-400, and SSV2

Link	OK	Mismatch	Missing
HMDB-Pantheon-1	0	1447	46
HMDB-Pantheon-2	0	1113	414
HMDB-Pantheon-3	0	1115	415
HMDB-Pantheon-4	0	1520	10
HMDB-Pantheon-5	0	1510	20
HMDB-Pantheon-6	0	1512	18
HMDB-Clean	1530	0	0
UCF-Pantheon-1	0	3712	17
UCF-Pantheon-2	0	3721	62
UCF-Pantheon-3	0	3718	63
UCF-Pantheon-4	0	3726	57
UCF-Pantheon-5	0	3715	68
UCF-Pantheon-6	0	3749	34
UCF-Clean	3783	0	0
Kinetics-Pantheon-1	0	15325	1972
Kinetics-Pantheon-2	0	155787	1719
Kinetics-Pantheon-3	0	15553	1744
Kinetics-Pantheon-4	0	17105	192
Kinetics-Pantheon-5	0	17075	222
Kinetics-Pantheon-6	0	17116	181
Kinetics-Clean	17297	0	0
SSV2-Pantheon-1	0	8467	16310
SSV2-Pantheon-2	0	7026	17751
SSV2-Pantheon-3	0	17870	6907
SSV2-Pantheon-4	0	24776	1
SSV2-Pantheon-5	0	24772	5
SSV2-Pantheon-6	0	24776	1
SSV2-Clean	24777	0	0

us to test the utility of data augmentation for visual artifacts and temporal truncation separately.

C.2 Results

C.2.1 File checksums

Table 31 shows that on all datasets, checksums result in clean videos being discarded indiscriminately, as all streamed videos are flagged as mismatched. This can happen if the streaming process changes the underlying bit-representation of the video without perceptible changes to visual video quality, i.e. under change of video container, different frame rate, or varying encoding parameters (compression quality).

Table 32: 3D-ResNet18 Accuracy under Networking Corruptions with Downsampled Videos, HMDB51

Link	96p	120p	144p	Original (240p)
Pantheon-1	50.9	51.4	55.2	43.3
Pantheon-2	57.0	48.6	50.4	37.7
Pantheon-3	56.5	53.8	49.9	43.7
Pantheon-4	60.6	57.6	60.4	64.2
Clean	61.4	60.2	61.5	64.8

Table 33: 3D-ResNet18 Accuracy with HEVC/H.265 Codec-based Streaming, HMDB51

Link	HEVC/H.265	Original (H.264)
Pantheon-1	38.8	43.3
Pantheon-2	37.6	37.7
Pantheon-3	28.1	43.7
Pantheon-4	61.3	64.2
Clean	61.8	64.8

C.2.2 Streaming with Downsampled Videos

Downsampling shows promise for mitigating some effects of corruption at the cost of clean-data accuracy. As seen in Table 32, evaluating on videos streamed at 144p, clean-data accuracy drops 4.0%, but accuracy improves on Pantheon-1, -2 and -3 up to 13.7% (Pantheon-2). At 120p and 96p, accuracy drops further on clean data and Pantheon-1, but improves Pantheon-2 accuracy up to another 3.6%. All models trained on downsampled videos perform better than the model trained on clean data. However, the model trained to recognize 120p videos performs worse than the model trained for 96p and 144p videos. We retained default hyperparameter settings for all videos; performance may improve with better hyperparameter tuning.

Downsampling may be successful as it lowers the bandwidth requirement for streaming. However, the accuracy drop on clean data suggests that the lower resolution also makes recognizing actions slightly harder. Thus, we conclude that downsampling is promising, but there remains a 10% gap to clean-data accuracy. We highlight that it is unclear whether the utility of downsampling will generalize to other video benchmarks that require finer-grained spatial reasoning; we leave this question to future work.

C.2.3 HEVC Codec

We found that streaming videos using the HEVC codec hurts accuracy on Pantheon 1, -2, and -3 up to 15.6% (Table 33). Interestingly, we found that the severity of video truncation worsened when using HEVC, as compared to H.264. For example, the median video length dropped to 0.07s on Pantheon-3 (compare: 1.38s, H.264 on Pantheon-3). We did not tune or experiment with codec parameters beyond the default settings, so we note that accuracy may improve with better codec settings.

Table 34: 3D-ResNet18 Accuracy with Adversarial Training, HMDB51

Link	$\varepsilon = 2$	$\varepsilon = 4$	$\varepsilon = 8$	Original
Pantheon-1	37.6	36.1	32.6	43.3
Pantheon-2	29.4	31.0	25.6	37.7
Pantheon-3	34.0	32.8	39.4	43.7
Pantheon-4	52.2	50.6	45.3	64.2
Pantheon-5	52.5	50.8	45.8	64.5
Pantheon-6	52.7	51.0	45.7	64.5
Clean	52.5	51.0	45.3	64.8

Table 35: 3D-ResNet18 Accuracy with Varying Training Window Size, HMDB51

Link	4-frame	8-frame	Original (16-frame)
Pantheon-1	19.0	24.7	43.3
Pantheon-2	15.2	17.5	37.7
Pantheon-3	20.0	23.7	43.7
Pantheon-4	23.9	31.9	64.2
Clean	25.0	34.7	64.8

C.2.4 Adversarial Training

Table 34 shows that adversarial training hurts model accuracy on both clean and networking-corrupted data. This effect is consistent across all Pantheon links. Furthermore, as perturbation budget ε increases, which corresponds to the maximum variation allowed in an adversarial example, the performance drop worsens as well. Again, this result suggests that the ℓ_p norm standard adversarial robustness framework is not applicable to networking corruptions due to its generality. This motivates the exploration of more targeted approaches to mitigating the impact of networking corruptions.

C.2.5 Decreased Training Window Size

We found that decreasing the video window size used during model training generally harms model performance. However, this lowers clean-data accuracy by 30.3% when the training video window size is decreased from 16 frames to either 8 or 4 frames (Table 35). The performance drop suggests that too much temporal information is removed. Clean-data accuracy may improve with further tuning, but we do not observe more robustness to truncation when using smaller training windows, since corrupt accuracy drops into the 20s on Pantheon-1, -2, and -3 in both the 4-frame and 8-frame configurations. Though our initial result is negative, learned frame samplers, which learn to select relevant frames instead of a fixed window, may be more suitable for improving robustness to truncation. We leave this as future work.

C.2.6 Out of Distribution Filtering

We find that using the ODIN out-of-distribution detection method as a filter before inference improves accuracy on corrupted HMDB51 by up to 16.7% (Pantheon-3), leaving a 4% gap to clean-data accuracy (Table 36). Performance on Pantheon-1 and -2 improves significantly as well, but still lags 12.3% and 12.5% respectively behind clean data accuracy. OOD also exhibits moderate

Table 36: 3D-ResNet18 with OOD Filtering and OOD Detection AUROC, HMDB51

Link	Acc. Post-OOD	OOD AUROC	Acc. w/o OOD
Pantheon-1	52.1	81.2	43.3
Pantheon-2	51.9	82.2	37.7
Pantheon-3	60.4	75.4	43.7
Pantheon-4	67.0	66.2	64.2
Clean	68.8	66.1	64.8

Table 37: 3D-ResNet18 Accuracy with Networking-Corruption Augmentation, HMDB51

Link	Augmented	No Augmentation
Pantheon-1	41.9	43.3
Pantheon-2	37.2	37.7
Pantheon-3	42.9	43.7
Pantheon-4	60.8	64.2
Clean	N/A	64.8

discriminatory performance, with AUROC ranging from 75.4 (Pantheon-3) to 82.2 (Pantheon-2). Concretely, when used on the clean dataset, this method discards 11.0% of clean videos (168 of 1530), which is more than double the expected false positive rate 5.0%. Thus, ODIN is promising in settings where filtering videos is possible. However, it remains prone to false positives on clean data.

C.2.7 Networking Corruption-Based Data Augmentation

We find that, while data augmentation is unsuccessful in restoring performance, that it can slightly mitigate the impact of severe packet loss, but not temporal truncation. This result suggests that temporal truncation makes classification under networking corruptions inherently more difficult. Intuitively, temporal truncation both decreases the amount of signal available for training, and may also induce label noise if the action of interest is lost.

Data Augmentation. Table 37 shows that data augmentation is insufficient to significantly improve corrupt accuracy on HMDB51. At best, on Pantheon-2, data augmentation improves performance by 0.7%. This suggests that data augmentation is insufficient to improve the robustness of video ML models to networking corruptions. Note that since videos corrupted by Pantheon-5, and -6 were nearly identical to those corrupted by Pantheon-4 on the action recognition task, we computed results for models augmented with networking-corrupted video from Pantheon-1 through

Table 38: 3D-ResNet18 Accuracy with Packet Loss Augmentation, HMDB51

Packet loss rate (%)	Augmented	No Augmentation
0.1	59.9	62.6
1	59.9	59.5
10	49.6	49.2
20	36.9	33.9
Clean	59.9	64.8

Table 39: 3D-ResNet18 Accuracy with Bandwidth Augmentation, HMDB51

Bandwidth (Mbps)	Augmented	No Augmentation
0.12	35.5	39.1
0.5	49.6	50.1
1	51.2	54.1
5	59.4	60.8
10	61.0	64.4
50	60.8	64.5
100	60.8	64.5
Clean	64.8	60.0

-4 only.

Packet-loss augmentation. For packet loss augmentation, we proceed with the data augmentation setup, except that we use videos corrupted at all levels of packet loss (0.1%, 1%, 10%, 20%). Table 38 shows that this scheme improves accuracy on highly-corrupted data (3.0%, 20% packet loss rate and 0.4%, 10% packet loss rate), but improvements taper off as packet loss rate decreases. This suggests that data augmentation might be somewhat effective against visual artifacts.

Bandwidth augmentation. For bandwidth augmentation, we proceed with the data augmentation setup, except that we use videos corrupted at varying bandwidth limits (0.12, 0.5, 1, 5, 10, 50, 100 Mbps). Table 39 shows that this scheme consistently harms model performance. Intuitively, bandwidth-based data augmentation results in truncated examples in the training dataset, which may drop important action information. Furthermore, sufficient levels of truncation may actually change the label of the underlying video if the relevant action is dropped from the video, introducing noise into the labels. This can break the assumption in data augmentation that the augmented video retains the same classification label.